Interplay between electronic correlation and atomic disorder in a low carrier density 4*d* transition-metal oxide

T. Yasuda,[1] Y. Kondo,[2] T. Kajita,[2] K. Murota,[1] D. Ootsuki,[3] Y. Takagi,[4] A. Yasui,[4] N. L. Saini,[5] T. Katsufuji,[2] and T. Mizokawa[1]

[1]*Department of Applied Physics, Waseda University, Shinjuku, Tokyo 169-8555, Japan*
[2]*Department of Physics, Waseda University, Shinjuku, Tokyo 169-8555, Japan*
[3]*Department of Interdisciplinary Environment, Kyoto University, Sakyo, Kyoto 606-8501, Japan*
[4]*Japan Synchrotron Radiation Research Institute, Sayo, Hyogo 679-5198, Japan*
[5]*Department of Physics, University of Roma "La Sapienza," Piazalle Aldo Moro 2, 00185 Rome, Italy*

(Received 26 May 2020; revised 12 October 2020; accepted 9 November 2020; published 30 November 2020)

We have investigated electronic structure evolution by cation substitution in $Ba_{3-x}Sr_xNb_5O_{15}$ by means of hard x-ray photoemission spectroscopy. Localization of Nb 4*d* electrons manifests as spectral weight transfer from a coherent component at the Fermi level to an incoherent one at 1–2 eV below it. This behavior is similar to that of electron-doped $SrTiO_3$. On the other hand, Nb 3*d* and 4*p* core level spectra exhibit a screening effect with an energy scale of 1–2 eV by the coherent Nb 4*d* electrons similar to 4*d* electron systems near Mott transitions. The energy scale indicates that electron correlation is involved in the metal to insulator transition in the present system, although the Nb 4*d* band is about 1/10 filled. The present results suggest a mechanism of electron localization due to atomic disorder and electron correlation.

DOI: 10.1103/PhysRevB.102.205133

I. INTRODUCTION

It is a challenging and fascinating task to understand metallic versus insulating behaviors of various transition-metal oxides with a partially filled *d* subshell in a systematic way since there are a variety of physical mechanisms of electron localization and delocalization [1,2]. In 3*d* transition-metal oxides, strong electron-electron interaction plays essential roles in realizing Mott insulators due to on-site Coulomb interaction and charge-ordered insulators due to intersite Coulomb interaction [1]. In addition to the electron-electron interaction, several transition-metal oxides such as VO_2 and $LiVO_2$ exhibit metal to insulator transitions driven by dimerization or trimerization through strong electron-lattice interaction [2,3]. Although 4*d* and 5*d* transition-metal oxides tend to be metallic due to larger *d* band width, some of the 4*d* and 5*d* transition-metal oxides such as Ca_2RuO_4 are insulators driven by a combination of electron-electron interaction and strong spin-orbit coupling [2,4]. When a small number of *d* electrons are introduced in d^0 systems such as $SrTiO_3$ and $KNbO_3$ [5,6], the transition-metal *d* band accommodates low-density carriers, which are highly mobile. On the other hand, it is also known that correlated *d* electrons coexist with the highly mobile *d* electrons and manifest as an incoherent spectral feature below the Fermi level in the case of electron-doped $SrTiO_3$ [5,7–9]. Compared to the 3*d* systems, electronic properties of 4*d* transition-metal oxides with low carrier density have not been studied well so far. In particular, considering the recent research interest in the spin-orbit coupled 4*d*/5*d* transition-metal compounds, coherent/incoherent spectral features in 4*d* systems would be highly interesting if they exist.

It has been pointed out that several early transition-metal oxides near metal to insulator transitions (including electron-doped $SrTiO_3$) commonly show a small thermal conductivity in the correlated metallic phase with strong lattice fluctuations [10]. The lattice fluctuations are associated with the existence of correlated *d* electrons in low carrier density systems. Among the early transition-metal oxides, $Ba_{3-x}Sr_xNb_5O_{15}$ is a unique 4*d* electron system with a metal to insulator transition by Sr substitution for Ba. While $Ba_{3-x}Sr_xNb_5O_{15}$ is a good metal with a partially filled Nb 4*d* band for $0 \leqslant x \leqslant 2$, it shows semiconducting or insulating behavior at low temperature for $x \geqslant 3$ [11,12]. As shown in Fig. 1, the NbO_6 octahedra share their corners and form a three-dimensional network [13–17]. The A-site (Ba or Sr) ions are surrounded by the NbO_6 octahedra in two different ways. The A1 site surrounded by eight NbO_6 octahedra has 12 nearest oxygen atoms. The A2 site is surrounded by ten NbO_6 octahedra, and six of them are rather closer to the A2 site than the others. The A2 site has nine nearest oxygen atoms, and the A2-O bond length tends to be longer than the A1-O bond length [13]. The tetragonal or orthorhombic unit cell includes two A1 sites and four A2 sites. It has been pointed out that the smaller Sr (larger Ba) ions tend to occupy the A1 (A2) site [13].

As for the mechanism of the metal to insulator transition, Kolodiazhnyi *et al.* have proposed Anderson-type electron localization due to intrinsic disorder by Sr substitution for larger Ba on the A2 crystallographic site, which is evidenced by the large atomic displacement parameters of the Sr and Nb ions [11]. Also the lattice thermal conductivity is suppressed for $x \geqslant 3$, suggesting structural disorder by Sr substitution for the A2 site [17]. In this context, it is highly interesting to study

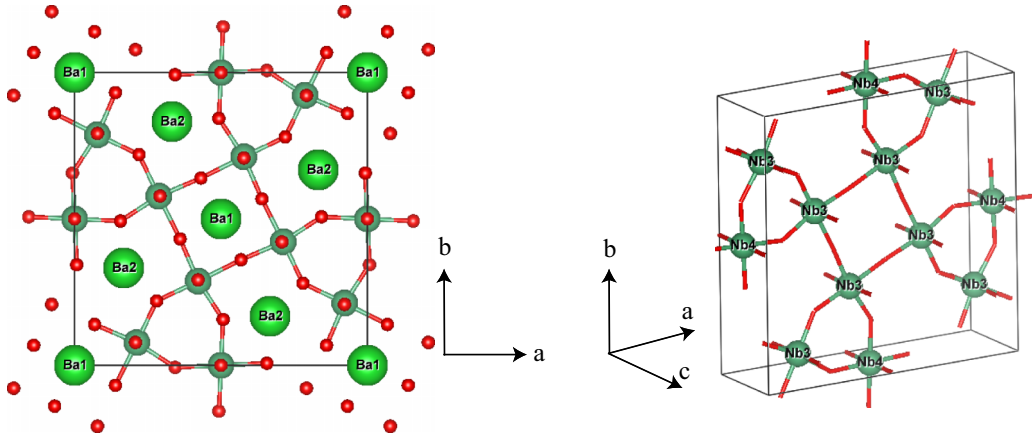

FIG. 1. Left: Crystal structure of $Ba_3Nb_5O_{15}$. Right: Nb-O network in $Ba_3Nb_5O_{15}$. The figures are created by VESTA [18].

the electronic and lattice properties of $Ba_{3-x}Sr_xNb_5O_{15}$ by means of spectroscopic methods and to compare them with those of 3*d* transition-metal oxides such as $La_{1-x}Sr_xTiO_3$. In the present work, we have performed hard x-ray photoemission spectroscopy (HAXPES) for single crystals of $Ba_{3-x}Sr_xNb_5O_{15}$ ($x = 0.0$, 1.0, 1.5, and 2.0) in order to observe the electronic structure evolution by Sr substitution for Ba. The present study has revealed that the moderately correlated Nb 4*d* electrons exhibit a unique spectral evolution driven by lattice disorder and electron-electron interaction.

II. EXPERIMENT

The single crystals are grown by the floating-zone method, which will be reported elsewhere [12]. HAXPES measurements were performed at BL47XU of SPring-8 [19,20] with 7940-eV photon energy, which has a probing depth of about 10 nm [21–24]. The x-ray incidence angle was 25°, and the photoelectron detection angle was 90°. The beam spot size was set to about $1 \times 5\ \mu m^2$. The typical size of the beam footprint on the samples was about $1 \times 12\ \mu m^2$. The single crystals were fractured under ultrahigh vacuum of 10^{-6} Pa at 300 K in order to avoid surface contamination. The measurements were performed at 300 K. Emitted photoelectrons were collected by the VG SCIENTA R4000-10kV analyzer. The pass energy was set to 200 eV, and the total energy resolution was about 270 meV. The binding energy of the HAXPES spectra was calibrated using the Fermi edge of Au.

III. RESULTS AND DISCUSSION

O 1*s* HAXPES spectra for $Ba_{3-x}Sr_xNb_5O_{15}$ ($x = 0.0$, 1.0, 1.5, and 2.0) are displayed in Fig. 2(a). The O 1*s* spectra of $x = 0.0$ showed position dependence, which could be detected due to the small spot size of $1 \times 5\ \mu m^2$ in the present measurement. The O 1*s* peak is located at 530.7 eV in region 1, while it is around 531.1 eV in region 2. The O 1*s* spectrum of region 1 agreed with those taken with a larger spot size, indicating that the spectrum of region 1 represents the bulk electronic state of $Ba_3Nb_5O_{15}$. The spectrum of region 2 suggests a secondary phase embedded in $Ba_3Nb_5O_{15}$ which would be associated with structural instability of $Ba_3Nb_5O_{15}$ due to occupation of the compact A1 site by relatively large Ba ions. This point will be discussed in the next paragraph based on Ba 5*p* spectra. Such a secondary phase is not detected in the Sr-substituted systems ($x = 1.0$, 1.5, and 2.0). This is probably because the Ba ions in the compact A1 site are replaced by relatively small Sr ions. The O 1*s* peak position of $Ba_2SrNb_5O_{15}$ is around 530.7 eV, which is consistent with region 1 of $Ba_3Nb_5O_{15}$. This observation supports the assignment of region 1 to the bulk $Ba_3Nb_5O_{15}$. With further Sr substitution, the O 1*s* binding energy gradually increases from 530.7 to 530.9 eV. The O 1*s* peaks are fitted to two Gaussian functions (peak 1 and peak 2) in order to analyze their asymmetric shape. The energy difference between peak 1 and peak 2 is about 0.7 eV for region 2 of $Ba_3Nb_5O_{15}$, while it is about 1.2 eV for the others. This indicates that the main reasons for the asymmetric shape are different between them. Most likely, the high binding energy component (peak 2) is derived from oxygen defects for region 2 of $Ba_3Nb_5O_{15}$, while the asymmetric shape is mainly due to the Doniach-Šunjić mechanism by conduction electrons for the others. Indeed, the relative intensity of peak 2, which is a measure of asymmetry, is reduced in less metallic $BaSr_2Nb_5O_{15}$, as shown in Fig. 2(b).

Figure 3 shows Ba 5*p*, Sr 4*p*, and O 2*s* peaks. The Ba 5*p* and Sr 4*p* contributions decrease and increase, respectively, with Sr substitution for Ba. Interestingly, the Ba $5p_{3/2}$ peak at 14.5 eV is accompanied by another peak at 13.8 eV for region 1 of $Ba_3Nb_5O_{15}$. The peaks at 14.5 and 13.8 eV can be assigned to Ba ions at the A2 and A1 sites, respectively. The peak at 13.8 eV rapidly loses its intensity by Sr substitution from $x = 0.0$ ($Ba_3Nb_5O_{15}$) to $x = 1.0$ ($Ba_2SrNb_5O_{15}$), while that at 14.5 eV keeps its intensity. For $x = 0.0$, Ba ions are surrounded by NbO_6 octahedra in two different ways. The Ba1 ions at the A1 site surrounded by eight NbO_6 octahedra have 12 nearest oxygen atoms. The Ba2 ions at the A2 site are surrounded by ten NbO_6 octahedra, and six of them are rather closer to the Ba2 ions than the others. The Ba2 ions have nine nearest oxygen atoms, and the Ba2-O bond length tends to be longer than the Ba1-O bond length [13]. Therefore, it is expected that smaller Sr ions tend to replace the Ba1 ions. Since the unit cell includes two Ba1 ions and four Ba2 ions, almost all the Ba1 ions are replaced by the Sr ions in going from $x = 0.0$ to 1.0. Indeed, the experimental result for the Ba 5*p* peak is consistent with this scenario. Interestingly, the

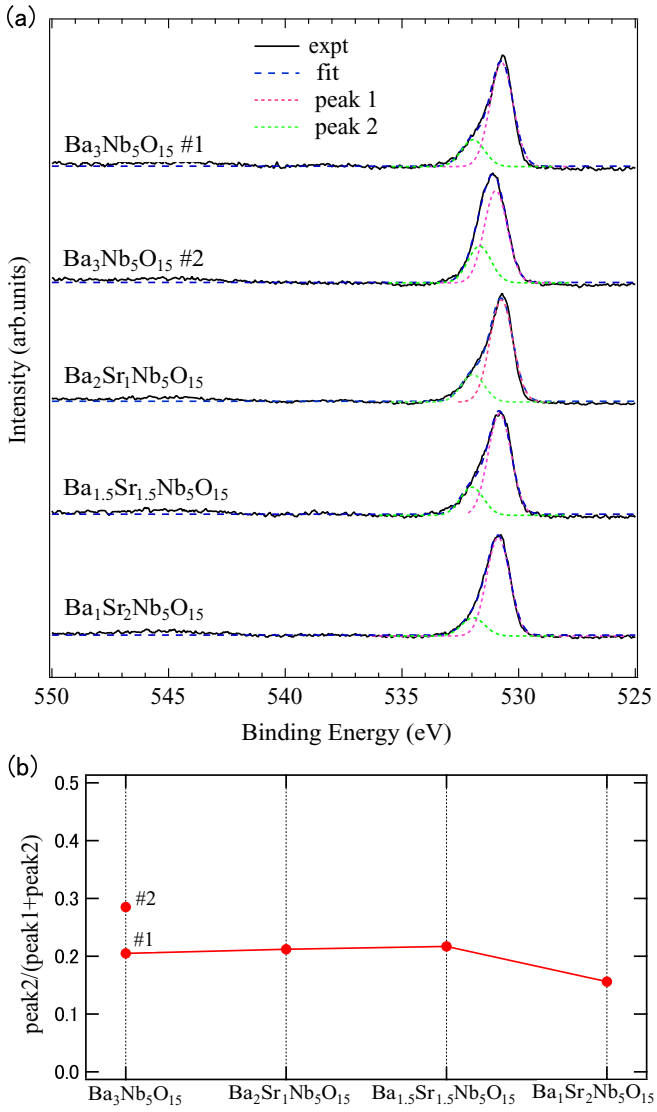

FIG. 2. (a) O 1*s* HAXPES of $Ba_{3-x}Sr_xNb_5O_{15}$ ($x = 0.0$, 1.0, 1.5, and 2.0) taken at room temperature. The spectrum labeled 1 represents the bulk electronic state of $Ba_3Nb_5O_{15}$, while that labeled 2 is assigned to a secondary phase embedded in $Ba_3Nb_5O_{15}$. The O 1*s* peak is fitted to two Gaussian functions (peak 1 and peak 2). (b) Ratio of the secondary Gaussian peak area (peak 2) to the total area (peak 1+peak 2).

peak at 13.8 eV for the Ba1 ions is almost absent in region 2 of $Ba_3Nb_5O_{15}$. Since the Ba1 ions at the compact A1 site are not favored, it is speculated that the Ba1 ions are removed and oxygen defects are created in the secondary phase (region 2) embedded in $Ba_3Nb_5O_{15}$. In the Sr-substituted systems, the secondary phase is not created since the Ba1 ions are replaced by smaller Sr ions. In going from $x = 1.0$ to 2.0, the Ba2 ions are replaced by Sr ions in addition to the Ba1 ions. Indeed, the Ba $5p_{3/2}$ peak at 14.5 eV gradually decreases from $x = 1.0$ to 2.0 in Fig. 3.

Figure 4 shows Nb 3*d* and Ba 4*p* HAXPES spectra for $Ba_{3-x}Sr_xNb_5O_{15}$ ($x = 0.0$, 1.0, 1.5, and 2.0). The broad Ba 4*p* contribution around 204 eV decreases with Sr substitution for Ba. In addition to the main Nb $3d_{5/2}$ and Nb $3d_{3/2}$ peaks,

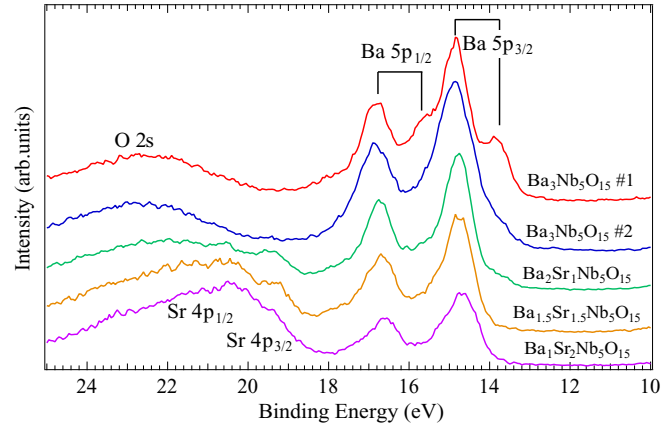

FIG. 3. Ba 5*p*, Sr 4*p*, and O 2*s* HAXPES spectra of $Ba_{3-x}Sr_xNb_5O_{15}$ ($x = 0.0$, 1.0, 1.5, and 2.0) taken at room temperature. The spectrum labeled 1 represents the bulk electronic state of $Ba_3Nb_5O_{15}$, while that labeled 2 is assigned to a secondary phase embedded in $Ba_3Nb_5O_{15}$.

shoulders are observed on the lower binding energy side, as indicated by arrows in Fig. 4. In the case of $La_{1-x}Sr_xTiO_3$ or electron-doped $SrTiO_3$, the low-energy shoulder is assigned to Ti^{3+} [5]. In the present case, the spectral weight of the low-energy shoulder is too large compared to the average Nb valence of +4.8. Also, it is inconsistent with the fact that the low-energy shoulder decreases with the Sr substitution, although the average Nb valence does not change. Instead of the Nb^{4+} contribution, the low-energy shoulder can be assigned to the screening effect by the Nb 4*d* conduction electrons since its spectral weight decreases in the insulating composition. Such a screening effect is commonly observed in various 4*d* transition-metal oxides with moderately correlated 4*d*

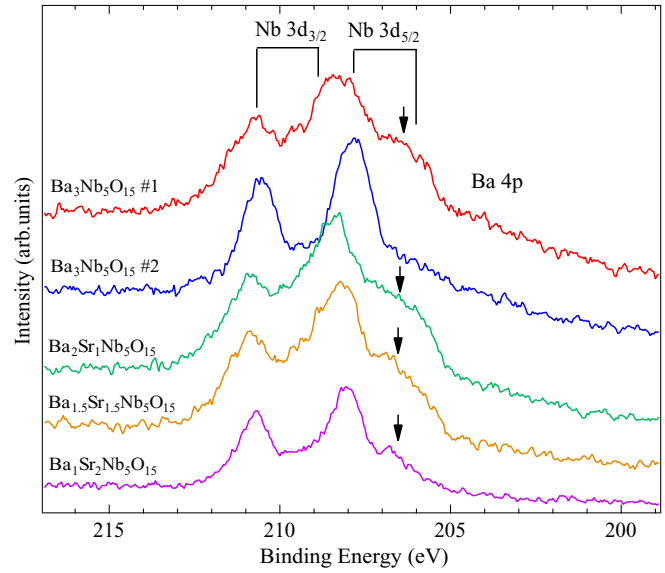

FIG. 4. Nb 3*d* HAXPES of $Ba_{3-x}Sr_xNb_5O_{15}$ ($x = 0.0$, 1.0, 1.5, and 2.0) taken at room temperature. The spectrum labeled 1 represents the bulk electronic state of $Ba_3Nb_5O_{15}$, while that labeled 2 is assigned to a secondary phase embedded in $Ba_3Nb_5O_{15}$. The arrows indicate low-energy shoulders for Nb $3d_{5/2}$.

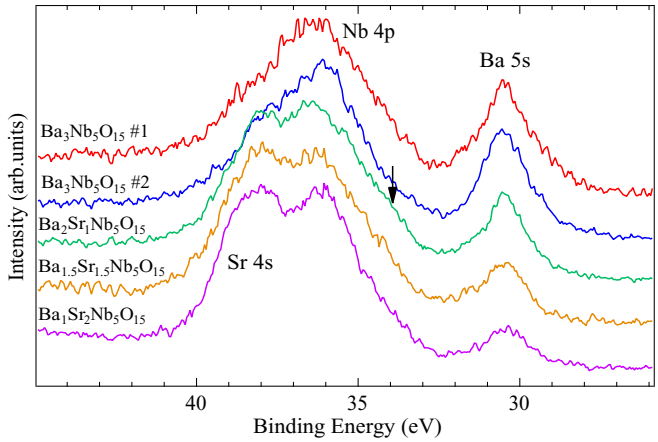

FIG. 5. Nb 4*p* HAXPES of $Ba_{3-x}Sr_xNb_5O_{15}$ ($x = 0.0$, 1.0, 1.5, and 2.0) taken at room temperature. The spectrum labeled 1 represents the bulk electronic state of $Ba_3Nb_5O_{15}$, while that labeled 2 is assigned to a secondary phase embedded in $Ba_3Nb_5O_{15}$. The arrow indicates a low-energy shoulder for Nb 4*p*.

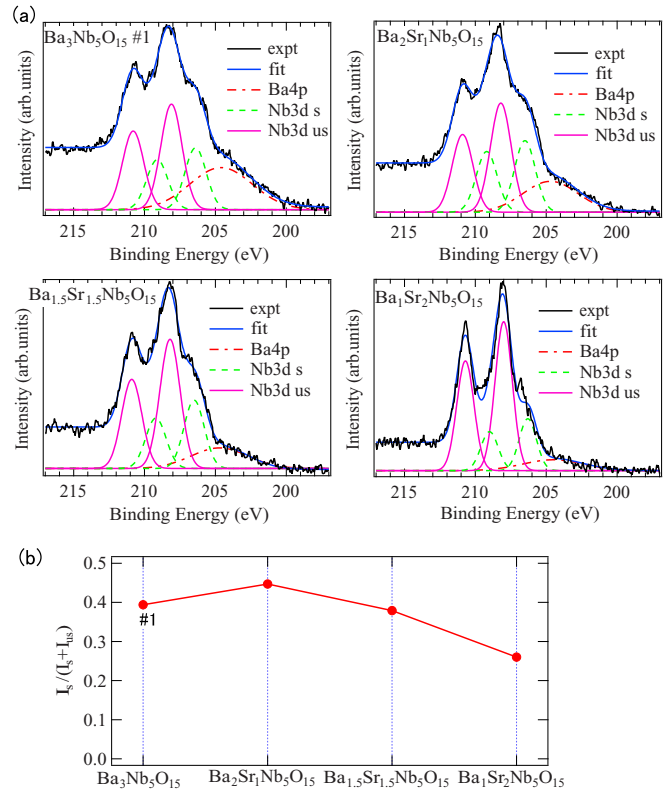

FIG. 6. (a) Decomposition of Nb 3*d* spectra into screened and unscreened peaks. (b) Ratio of the screened peak area relative to the total area of the screened and unscreened peaks of Nb 3*d* in $Ba_{3-x}Sr_xNb_5O_{15}$ ($x = 0.0$, 1.0, 1.5, and 2.0).

electrons such as $Ca_{2-x}Sr_xRuO_4$ [25–28]. For $x = 0.0$, the shoulder is intense in region 1, while it is relatively small in region 2. The situation in region 2 is similar to insulating Ca_2RuO_4 [25]. Most likely, the Nb 4*d* conduction electrons are localized or reduced in region 2. The binding energy of the main Nb $3d_{5/2}$ peak is larger in region 1 than that in region 2. It seems that, due to the existence of the low-energy shoulder (screened component), the main peak (unscreened component) is shifted to the higher binding energy side.

Figure 5 shows Nb 4*p* HAXPES spectra with contributions from Ba 5*s* and Sr 4*s*. The Ba 5*s* contribution decreases, and the Sr 4*s* contribution increases with Sr substitution for Ba. In $Ba_2SrNb_5O_{15}$, the Nb 4*p* main peak is accompanied by a shoulder on the lower binding energy side, as indicated by the arrow in Fig. 5. Such shoulders are not clear in other compositions. However, compared to region 2, the Nb 4*p* peak has a tail on the low-energy side in region 1 of $Ba_3Nb_5O_{15}$, in $Ba_{1.5}Sr_{1.5}Nb_5O_{15}$, and in $BaSr_2Nb_5O_{15}$. Similar to the shoulders in the Nb 3*d* spectra, the shoulders or tails in the Nb 4*p* spectra can be assigned to the screening effect by Nb 4*d* conduction electrons. The Nb 3*d* and 4*p* core levels commonly show the screening effect with an energy scale of ~2 eV, which is similar to the screening effect in various 4*d* electron systems such as $Ca_{2-x}Sr_xRuO_4$ and $Y_{2-x}Bi_xRu_2O_7$ [25–28]. The shoulder structure in the core level spectra disappears if these 4*d* systems undergo Mott transitions and become Mott insulators. Therefore, it is expected that the Nb 4*d* electrons in $Ba_{3-x}Sr_xNb_5O_{15}$ have an electron correlation effect in a manner similar to $Ca_{2-x}Sr_xRuO_4$ and $Y_{2-x}Bi_xRu_2O_7$ in proximity to Mott transitions. The screening effect in $Ba_3Nb_5O_{15}$ is comparable to that for $W/U = 1.0$, where W and U are bandwidth and on-site Coulomb interaction, respectively [25].

The screening effect on the Nb 3*d* core hole is analyzed by fitting the spectra to Gaussian functions with a Shirley-type background [29], as shown in Fig. 6(a). Here, each of the Nb $3d_{5/2}$ and $3d_{3/2}$ peaks is decomposed into the screened and unscreened components. The ratio between the screened and unscreened components is assumed to be the same between the Nb $3d_{5/2}$ and $3d_{3/2}$ peaks. The screened spectral weight relative to the total spectral weight is plotted as a function of Sr substitution in Fig. 6(b). The screened spectral weight is about 0.4 for the metallic compositions ($x = 1.0$ and 1.5), while it is reduced to about 0.25 in the insulating composition ($x = 2.0$). This behavior is very similar to that observed in various Ru oxides near the Mott transition [25–28].

Figure 7 shows the valence band HAXPES spectra. For $x = 0.0$, the Nb 4*d* band is located at the Fermi level, as expected from its metallic property. The intensity at the Fermi level is much stronger in region 1 than in region 2. Instead, the intensity around 1.5 eV below the Fermi level is enhanced in region 2, which can be assigned to localized Nb 4*d* electrons. The integrated spectral weight from the Fermi level to 2 eV does not change substantially between the two regions. This result indicates that the number of Nb 4*d* electrons is similar between them. Assuming Ba^{2+}, Sr^{2+}, and O^{2-}, the average valence of Nb is estimated to be +4.8. Therefore, the formula unit with five Nb sites includes one Nb 4*d* electron. Most likely, the Nb 4*d* band width is reduced by local lattice disorder (which is indicated by the absence of the Ba1 ions in region 2), and the Nb 4*d* electrons are localized in region 2. This speculation is consistent with the absence of a shoulder structure in the Nb 3*d* and 4*p* core level spectra for region 2.

As for the Sr-substituted systems, the Nd 4*d* spectral weight at the Fermi level remains large from $x = 0.0$ to 1.0, which is consistent with the metallic transport behavior and

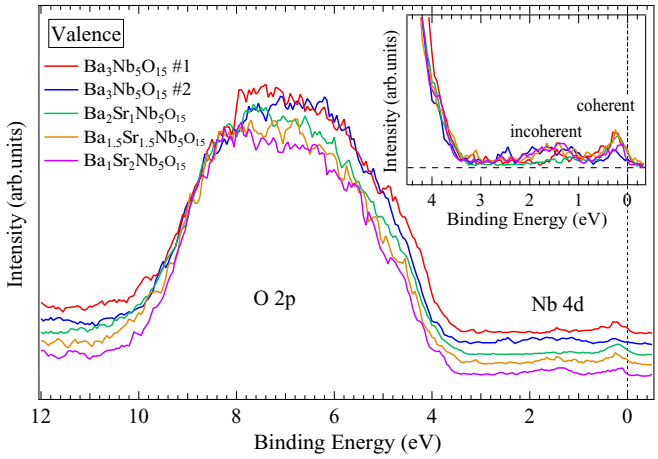

FIG. 7. Valence band HAXPES of $Ba_{3-x}Sr_xNb_5O_{15}$ ($x = 0.0$, 1.0, 1.5, and 2.0) taken at room temperature. The spectrum labeled 1 represents the bulk electronic state of $Ba_3Nb_5O_{15}$, while that labeled 2 is assigned to a secondary phase embedded in $Ba_3Nb_5O_{15}$. The inset shows the spectra near the Fermi level.

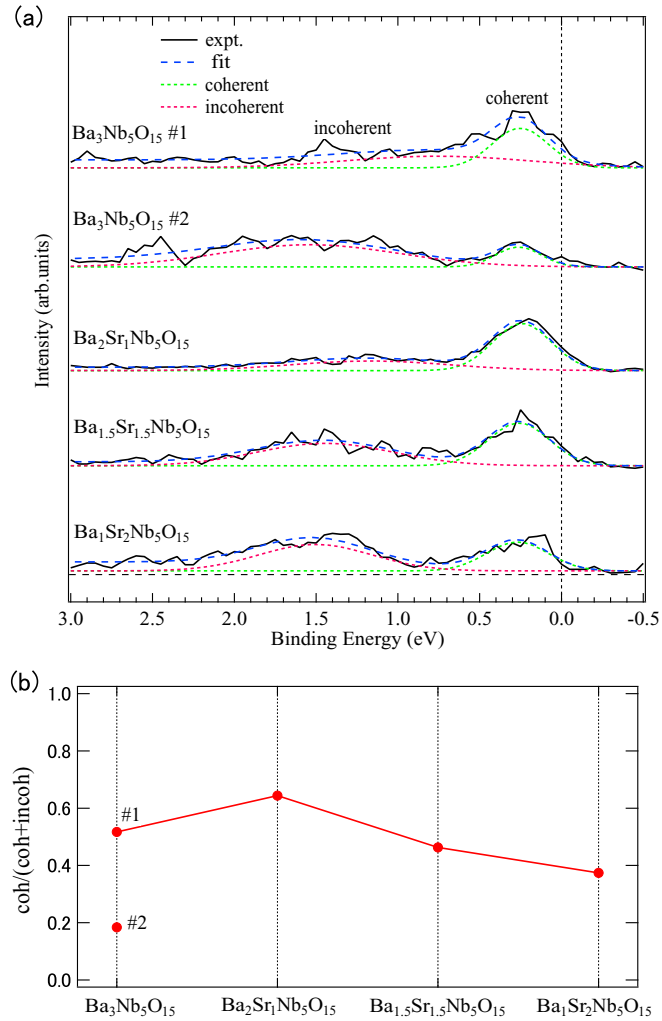

FIG. 8. (a) Nb 4*d* spectra fitted to two Gaussian functions and Shirley-type background. The two Gaussian functions correspond to the coherent and incoherent peaks. (b) Ratio of the coherent peak area relative to the total area of the coherent and incoherent peaks of Nb 4*d* in $Ba_{3-x}Sr_xNb_5O_{15}$ ($x = 0.0$, 1.0, 1.5, and 2.0).

the intense shoulder structure in the Nb 3*d* and 4*p* core level spectra. The Nd 4*d* spectral weight at the Fermi level is slightly reduced, and the 1.5 eV spectral weight is enhanced for $x = 1.5$. The Nd 4*d* spectral weight at the Fermi level is reduced further at $x = 2.0$. The integrated spectral weight from the Fermi level to 2 eV does not change substantially between $x = 0.0$ and 2.0, indicating that the metal to insulator transition is not caused by depletion of Nb 4*d* electrons. In order to estimate spectral weight of the coherent (at the Fermi level) and incoherent (at the higher binding energy) components, the Nb 4*d* spectra are fitted to two Gaussian functions and a Shirley-type background [29], as shown in Fig. 8(a). In going from $x = 1.0$ to 2.0, the spectral weight of the coherent part $I_{\rm coh}$ in the total Nb 4*d* spectral weight ($I_{\rm coh} + I_{\rm incoh}$, where $I_{\rm incoh}$ is the spectral weight of the incoherent part) decreases from 0.6 to 0.4, as shown in Fig. 8(b). This behavior is similar to that reported in $La_{1-x}Sr_xTiO_3$ or electron-doped $SrTiO_3$ [5], although the behavior of the core level spectra is different between the present Nb oxide and electron-doped $SrTiO_3$. The incoherent spectral weight represents partial localization of Nb 4*d* electrons, which is probably triggered by the atomic disorder, as indicated by the reduction in lattice thermal conductivity for $x \geqslant 1.5$ [11]. However, the coherent/incoherent features are not expected in a conventional Anderson localized state. Under the conventional Anderson localization, a disordered and localized band is located around the Fermi level, and a soft gap would be formed at the Fermi level due to long-range Coulomb interaction [30]. In the present system, once the 4*d* electrons are localized, the electronic correlation manifests as the separation between the coherent and incoherent peaks and the separation between the screened and unscreened peaks in the core level spectra. Such unusual spectral behavior may indicate a mechanism of metal to insulator transition driven by the combination of atomic disorder indicated by Kolodiazhnyi *et al.* [11] and electron correlation indicated by the present work. In order to describe such a correlated state with 1/10 electron filling, we need to go beyond Hubbard-like models and to include the long-range Coulomb interaction and the disordered lattice. Recently, a theory on cluster Mott insulators was developed by Chen, Kee, and Kim for $LiZn_2Mo_3O_8$ for a 1/6 electron filling kagome lattice [31]. Another related issue is the idea of the Wigner-Mott transition proposed by Li and Wang [32], which would be associated with the Mott insulating state in twisted bilayer graphene [33]. It is highly interesting whether spectral behaviors of such advanced models will be theoretically investigated and will be compared with the present experimental results.

As clarified by the Ba 5*p* and Sr 4*p* core level spectra in Fig. 5, only the A1 site with small A-O distance is occupied by the small Sr ions for *x* smaller than 1.0. Therefore, local lattice distortion due to Sr substitution is relatively small. When *x* becomes larger than 1.0, the A2 site with large A-O distance is occupied by the small Sr ions. Consequently, strong atomic disorder is introduced at the A2 site where the Sr ions have longer and weaker Sr-O bonds. The Sr ions may oscillate in the relatively large oxygen cage surrounding the A2 site and may produce nearly localized phonon modes (a kind of

rattling behavior) to reduce the lattice thermal conductivity. Such atomic disorder affects the NbO_6 octahedra which are responsible for the electronic transport properties. Here, we speculate that, since the number of 4*d* electrons per unit cell (including five Nb sites) is close to unity in the present system, the Nb 4*d* electrons localized by atomic disorder may resemble the Mott behavior which is usually expected for an integer number of electrons per site.

IV. CONCLUSION

In conclusion, we have performed a HAXPES study of $Ba_{3-x}Sr_xNb_5O_{15}$ in which the Sr substitution for Ba induces a metal to insulator transition. The transition manifests as Nb 4*d* spectral weight transfer from the coherent component at the Fermi level to the incoherent one at 1–2 eV below the Fermi level. The Nb 3*d* and 4*p* core level spectra are accompanied by a shoulder structure on the lower binding energy side which can be assigned to the screening effect by the coherent Nb 4*d* electrons. The Nb 4*d* spectral weight transfer and the screening effect in the core level spectra are very similar to those observed in 4*d* electron systems near Mott transitions. The energy scale of 1–2 eV indicates that electron correlation is involved in the metal to insulator transition in the present system, although the number of 4*d* electrons per Nb site is about 0.2. The present HAXPES study suggests a mechanism of metal to insulator transition which is driven by collaboration between atomic disorder and electron correlation.

ACKNOWLEDGMENTS

This work was supported by CREST-JST (Grant No. JPMJCR15Q2) and KAKENHI from JSPS (Grant No. 19H01853). The synchrotron radiation experiment was performed with the approval of SPring-8 (2017B1034, 2018A1012, 2019B1574). This work was supported by the joint research program of ZAIKEN, Waseda University (Project No. 31010).

[1] M. Imada, A. Fujimori, and Y. Tokura, Rev. Mod. Phys. **70**, 1039 (1998).
[2] D. I. Khomskii, *Transition Metal Compounds* (Cambridge University Press, Cambridge, 2014).
[3] Z. Hiroi, Prog. Solid State Chem. **43**, 47 (2015).
[4] T. Mizokawa, J. Electron Spectrosc. Relat. Phenom. **208**, 78 (2016).
[5] A. Chikina, F. Lechermann, M.-A. Husanu, M. Caputo, C. Cancellieri, X. Wang, T. Schmitt, M. Radovic, and V. N. Strocov, ACS Nano **12**, 7927 (2018).
[6] G. Li, H. Huang, S. Peng, Y. Xiong, Y. Xiao, S. Yan, Y. Cao, M. Tang, and Z. Li, RSC Adv. **9**, 35499 (2019).
[7] M. Takizawa, H. Wadati, K. Tanaka, M. Hashimoto, T. Yoshida, A. Fujimori, A. Chikamatsu, H. Kumigashira, M. Oshima, K. Shibuya, T. Mihara, T. Ohnishi, M. Lippmaa, M. Kawasaki, H. Koinuma, S. Okamoto, and A. J. Millis, Phys. Rev. Lett. **97**, 057601 (2006).
[8] Y. Ishida, R. Eguchi, M. Matsunami, K. Horiba, M. Taguchi, A. Chainani, Y. Senba, H. Ohashi, H. Ohta, and S. Shin, Phys. Rev. Lett. **100**, 056401 (2008).
[9] X. Hao, Z. Wang, M. Schmid, U. Diebold, and C. Franchini, Phys. Rev. B **91**, 085204 (2015).
[10] T. Katsufuji, T. Okuda, R. Murata, T. Kanzaki, K. Takayama, and T. Kajita, J. Phys. Soc. Jpn. **85**, 013703 (2016).
[11] T. Kolodiazhnyi, H. Sakurai, M. Isobe, Y. Matsushita, S. Forbes, Y. Mozharivskyj, T. J. S. Munsie, G. M. Luke, M. Gurak, and D. R. Clarke, Phys. Rev. B **92**, 214508 (2015).
[12] Y. Kondo, T. Kajita, and T. Katsufuji (unpublished).
[13] P. B. Jamieson, S. C. Abrahams, and J. L. Bernstein, J. Chem. Phys. **48**, 5048 (1968).
[14] B. Hessen, S. A. Sunshine, T. Siegrist, A. T. Fiory, and J. V. Waszczak, Chem. Mater. **3**, 528 (1991).
[15] B. Hessen, S. A. Sunshine, T. Siegrist, and R. Jimenez, Mater. Res. Bull. **26**, 85 (1991).
[16] Y. K. Hwang and Y.-U. Kwon, Mater. Res. Bull. **32**, 1495 (1997).
[17] T. Kolodiazhnyi, H. Sakurai, O. Vasylkiv, H. Borodianska, and Y. Mozharivskyj, Appl. Phys. Lett. **104**, 111903 (2014).
[18] K. Momma and F. Izumi, J. Appl. Crystallogr. **44**, 1272 (2011).
[19] E. Ikenaga, M. Kobata, H. Matsuda, T. Sugiyama, H. Daimon, and K. Kobayashi, J. Electron Spectrosc. Relat. Phenom. **190**, 180 (2013).
[20] E. Ikenaga, A. Yasui, N. Kawamura, M. Mizumaki, S. Tsutsui, and K. Mimura, Synchrotron Radiat. News **31**, 10 (2018).
[21] S. Ouardi, G. H. Fecher, and C. Felser, J. Electron Spectrosc. Relat. Phenom. **190**, 249 (2013).
[22] K. Kobayashi, M. Yabashi, Y. Takata, T. Tokushima, S. Shin, K. Tamasaku, D. Miwa, T. Ishikawa, H. Nohira, T. Hattori, Y. Sugita, O. Nakatsuka, A. Sakai, and S. Zaima, Appl. Phys. Lett. **83**, 1005 (2003).
[23] K. Kobayashi, Nucl. Instrum. Methods Phys. Res., Sect. A **601**, 32 (2009).
[24] K. Kobayashi, Nucl. Instrum. Methods Phys. Res., Sect. A **547**, 98 (2005).
[25] H.-D. Kim, H.-J. Noh, K. H. Kim, and S.-J. Oh, Phys. B (Amsterdam, Neth.) **359–361**, 1267 (2005).
[26] Z. V. Pchelkina, I. A. Nekrasov, T. Pruschke, A. Sekiyama, S. Suga, V. I. Anisimov, and D. Vollhardt, Phys. Rev. B **75**, 035122 (2007).
[27] G. Zhang and E. Pavarini, Phys. Rev. B **95**, 075145 (2017).
[28] A. Chikamatsu, Y. Kurauchi, K. Kawahara, T. Onozuka, M. Minohara, H. Kumigashira, E. Ikenaga, and T. Hasegawa, Phys. Rev. B **97**, 235101 (2018).
[29] D. A. Shirley, Phys. Rev. B **5**, 4709 (1972).
[30] A. L. Efros and B. I. Shklovskii, J. Phys. C **8**, L49 (1975).
[31] G. Chen, H.-Y. Kee, and Y. B. Kim, Phys. Rev. B **93**, 245134 (2016).
[32] C. Li and Z. Wang, Phys. Rev. B **80**, 125130 (2009).
[33] Y. Cao, V. Fatemi, A. Demir, S. Fang, S. L. Tomarken, J. Y. Luo, J. D. Sanchez-Yamagishi, K. Watanabe, T. Taniguchi, E. Kaxiras, R. C. Ashoori, and P. Jarillo-Herrero, Nature (London) **556**, 80 (2018).